

# Final Technical Report

## Refining Slip Rates and Earthquake Recurrence Times Along the San Andreas Fault Using Geodetic Data and 3D Viscoelastic Cycle Models

External Program Grant Number USGS # 05HQGR0021

Paul Segall  
Department of Geophysics  
Stanford University  
397 Panama Mall  
Stanford, CA 94305-2215  
Phone: (650) 725-7241  
Email: segall@stanford.edu

Kaj M. Johnson  
Department of Geological Sciences  
Indiana University  
1001 E. 10th St.  
Bloomington, IN 47405  
Phone: (812) 855-3612  
Email: kajjohns@indiana.edu

### Abstract

We develop a Bayesian inversion of GPS and geologic data for timing of past earthquakes, fault slip rates, and first-order lithosphere rheology in the San Francisco Bay Area. We determine the extent to which estimates of slip rates and recurrence times of large earthquakes obtained from geologic and paleoseismic data can be refined with geodetic data and a mechanical model. To do this, we construct a new 3D viscoelastic earthquake cycle model that consists of blocks bounded by faults in an elastic lithosphere overlying a

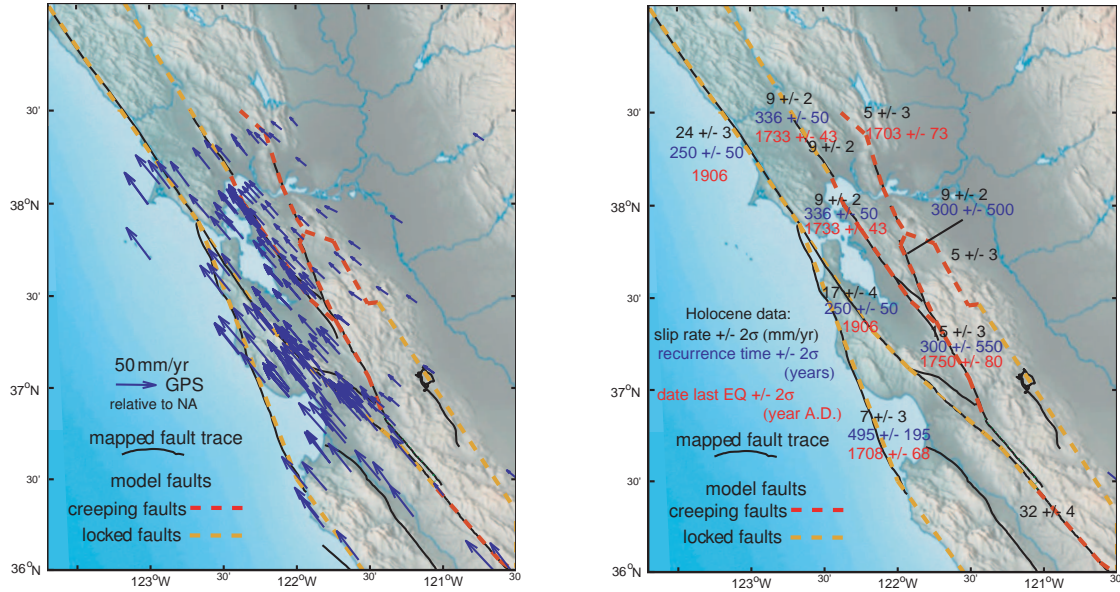


Figure 1: GPS and geologic data used in this study.

viscoelastic asthenosphere. A “steady-state” deformation field is assumed to exist in the absence of fault locking. Interseismic deformation is modeled as a perturbation to the steady-state due to backslip on locked portions of faults and viscous flow in the asthenosphere in response to past earthquakes. In this new model, the steady-state incorporates some accumulation of strain within the blocks near the bounding faults due to dip-slip motion on thrust faults and non-planar fault geometry. Incorporating geologic and paleoseismic estimates as formal priors, we invert Bay Area GPS and triangulation data for Euler pole locations (which determines slip rates), earthquake recurrence times, times since the last earthquake, asthenosphere viscosity, and lithosphere thickness. The inversion generally refines the geologic and paleoseismic estimates of slip rates and recurrence times, as indicated by posterior  $2\sigma$  uncertainties that are about half as large as prior uncertainties. Slip rates are generally consistent with geologic estimates. Recurrence times are not as well resolved as slip rates, but the inversion does provide an indication of whether recurrence times are relatively long ( $>500$  years) or short ( $<500$  years).

## Data

The data used in this study are shown in figures 1 and 2. The geologic data are implemented as prior prior probability distributions on fault slip rate and recurrence time assuming Gaussian distributions with mean and standard deviation given in figure 1.

As shown in figure 3, we partition the Bay Area faults into segments that rupture periodically in earthquakes with uniform slip.

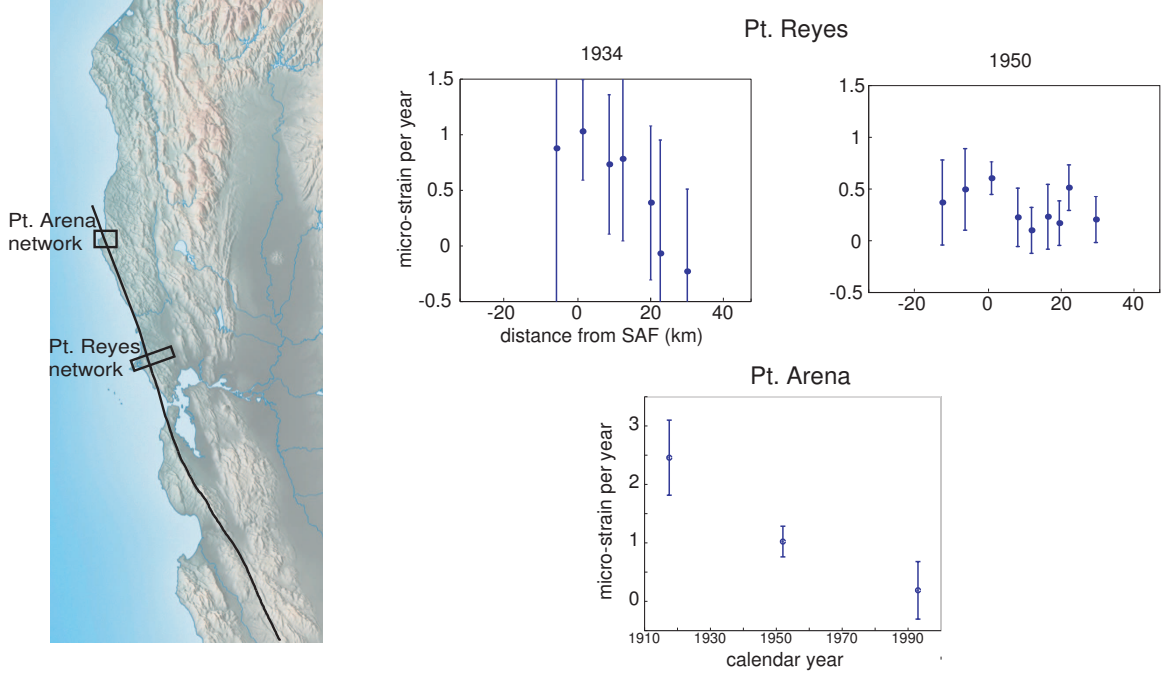


Figure 2: Triangulation data at Pt. Reyes and Pt. Arena.

## Viscoelastic Block Model

We construct a viscoelastic block model by extending the approach of elastic block models developed by Brendan Meade and Brad Hager and Robert McCaffrey. The forward model is similar to the 3D elastic block models conceived by Meade and Hager, McCaffrey, and Murray and Segall. The 3D elastic block models are a generalization of the 2D backslip model constructed by Savage. In the elastic block models a “steady state” is imagined in which blocks bounded by faults rotate on the surface of the earth about an Euler pole. In the absence of locking on the faults, the blocks translate undeformed. Elastic distortion due to locking of the faults is introduced with backslip on the faults. Sections of the fault that are completely locked are assigned backslip at the long-term rate. Sections that are creeping are assigned a backslip rate that is lower than the long-term rate. The elastic block models assume no long-term vertical motion which is problematic for areas with reverse faulting.

This 3D viscoelastic cycle model also uses the concept of a “steady-state” deformation in the absence of fault locking and backslip to construct the interseismic deformation field, but the “steady-state” does not consist of undeformed translating blocks. The “steady-state” model incorporates long-term distortion of the blocks near the bounding faults due to dip-slip motion on thrust faults and non-planar fault geometry. The steady-state velocity field is decomposed into three components as illustrated in Figure 4. We begin with far-field motion due to relative plate velocities. This motion assumes rigid-body rotations about an Euler pole (no vertical motion). For vertical faults bounding the rigid blocks, the rigid rotations lead to strike-slip and fault-normal discontinuities in the velocity field across the faults. Rigid-body rotations of blocks bounded by dipping faults

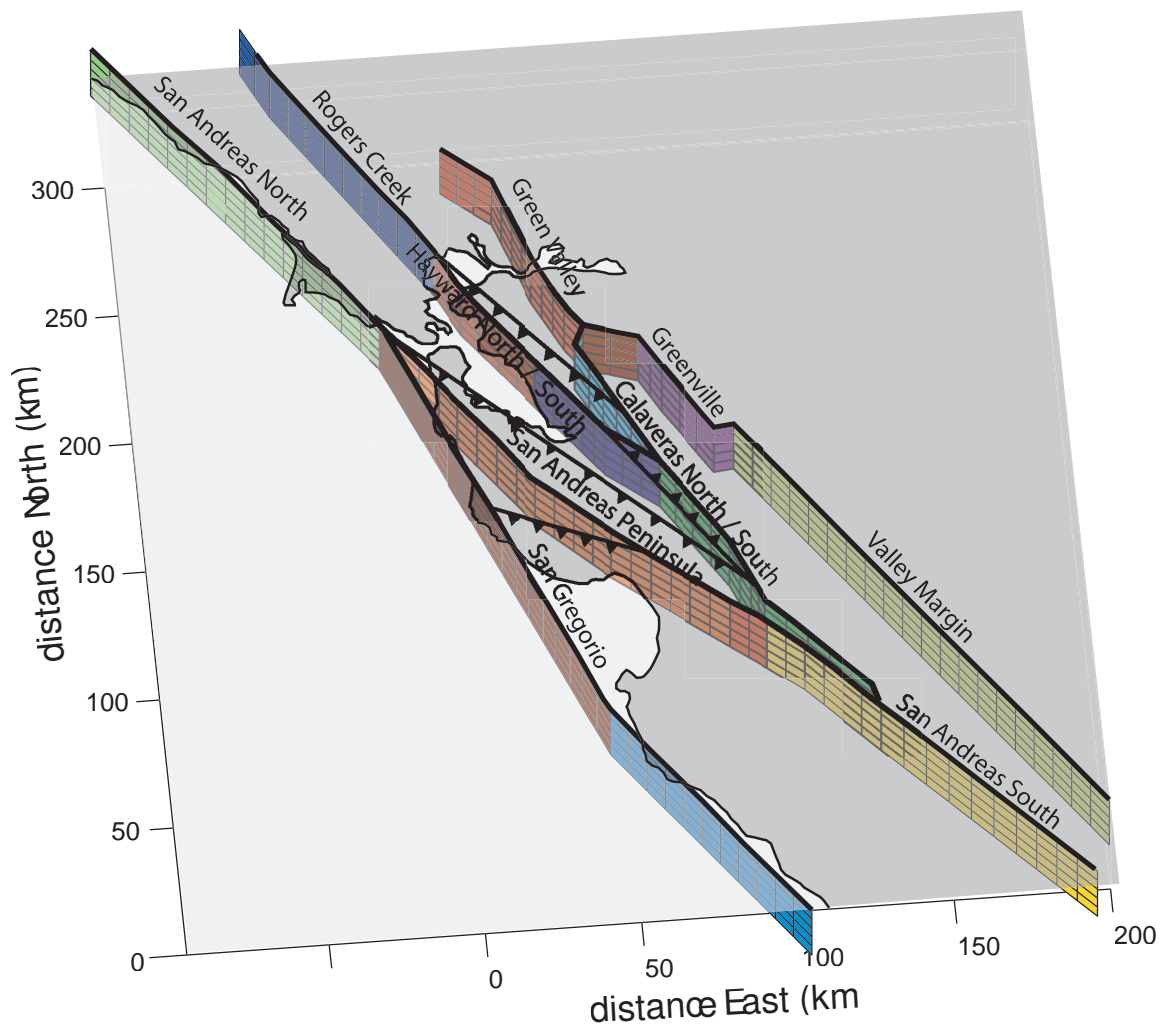


Figure 3: Fault geometry and segmentation assumed for this study.

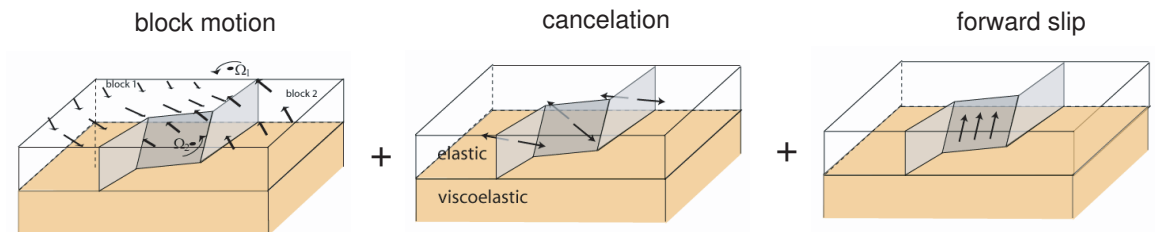


Figure 4: Illustration of the construction of the steady-state velocity field.

would lead in general lead to dip-slip, strike-slip, and tensile discontinuities across the faults. There are two problems with this steady-state velocity field. For one, the tensile discontinuity across faults is unphysical. Secondly, this model assumes no long-term vertical motion along dipping faults with dip-slip component - this is reasonable perhaps for subduction zones, but not for other settings. We therefore alter the rigid-body motion locally, near the faults, by a) forward slipping the dip-slip faults, and b) cancelling fault-normal discontinuities across all faults with tensile dislocations with sign opposite to the relative motion across the faults. The steady-state dip-slip motion on faults produces localized steady-state (long-term) vertical motions and long-term horizontal strain near dip-slip faults.

To obtain the interseismic velocity field, we perturb the steady-state velocity field by summing the contribution from backslip on locked sections of the faults and periodic forward slip to represent earthquakes.

## Bayesian mixed linear/nonlinear inversion

There are a large number of model parameters in this inversion. However, all of the Euler pole parameters are linearly related to the observations, and for a given set of nonlinear parameters, we can utilize least squares to estimate the Euler poles. We developed a mixed linear/nonlinear inversion scheme to take advantage of least squares.

### Forward model

Let  $\mathbf{d}_{gps}$  be  $N_{gps}$ -dimensional data vector of GPS velocities and let  $\mathbf{d}_{tri}$  be and  $N_{tri}$ -dimensional data vector of strain rates calculated from the triangulation data. Let  $\mathbf{m}$  be an  $M$ -dimensional vector of all the model parameters that are nonlinearly related to the surface observations. The observation equation is give by

$$\begin{pmatrix} \mathbf{d}_{gps} \\ \mathbf{d}_{tri} \end{pmatrix} = \begin{pmatrix} \mathbf{G}_{gps}(\mathbf{m}) \\ \mathbf{G}_{tri}(\mathbf{m}) \end{pmatrix} \Omega + \begin{pmatrix} \epsilon_{gps} \\ \epsilon_{tri} \end{pmatrix}, \quad \epsilon_{gps} \sim N(\mathbf{0}, \sigma_{gps}^2 \mathbf{\Sigma}_{gps}), \epsilon_{tri} \sim N(\mathbf{0}, \sigma_{tri}^2 \mathbf{\Sigma}_{tri}) \quad (1)$$

where  $\mathbf{G}_{gps}$  is an  $N_{gps} \times M$  matrix,  $\mathbf{G}_{tri}$  is and  $N_{tri} \times M$  matrix, and  $\epsilon_{gps}$  and  $\epsilon_{tri}$  are are vectors of observation error which is assumed to follow a Gaussian distribution with zero mean and covariance matrix of  $\sigma_{gps}^2 \mathbf{\Sigma}_{gps}$  and  $\sigma_{tri}^2 \mathbf{\Sigma}_{tri}$ . Here  $\sigma_{gps}^2$  and  $\sigma_{tri}^2$  are an unknown scale factors of the covariance matrices that account for the relative weighting of the data sets and unknown model variance.

### Bayesian formulation

We adopt a Bayesian approach to estimate  $\mathbf{m}$ ,  $\Omega$ ,  $\sigma_{gps}^2$ , and  $\sigma_{tri}^2$ . In the Bayesian approach, the solution to the inverse problem is the joint posterior probability density of the unknown parameters given data,  $p(\mathbf{m}, \Omega, \sigma_{gps}^2, \sigma_{tri}^2 | \mathbf{d}_{gps}, \mathbf{d}_{ti})$ . The linear and the non-linear parameters in the joint posterior distribution can be separated using an identity for joint probability:

$$p(\mathbf{m}, \Omega, \sigma_{gps}^2, \sigma_{tri}^2 | \mathbf{d}_{gps}, \mathbf{d}_{ti}) = p(\Omega | \mathbf{d}_{gps}, \mathbf{d}_{ti}, \mathbf{m}, \sigma_{gps}^2, \sigma_{tri}^2) p(\mathbf{m}, \sigma_{gps}^2, \sigma_{tri}^2 | \mathbf{d}_{gps}, \mathbf{d}_{ti}). \quad (2)$$

The first distribution of the right hand side,  $p(\Omega|\mathbf{d}_{gps}, \mathbf{d}_{ti}, \mathbf{m}, \sigma_{gps}^2, \sigma_{tri}^2)$ , is a Gaussian distribution because  $\mathbf{m}$ ,  $\sigma_{gps}^2$ , and  $\sigma_{tri}^2$  are specified, and therefore can be estimated with least squares. The second distribution of the right hand side,  $p(\mathbf{m}, \sigma_{gps}^2, \sigma_{tri}^2|\mathbf{d}_{gps}, \mathbf{d}_{ti})$ , is a non-Gaussian distribution and consequently cannot be estimated analytically. We employ a Markov chain Monte Carlo (MCMC) method to generate samples from the second distribution. We have a paper in preparation on the details of this method.

## Inversion Results

Figure 5 summarizes the inversion results for fault slip rate. The blue curves are the posterior distributions and the red vertical lines are the  $2\sigma$  interval of the prior distribution. The posterior distributions for elastic thickness, relaxation time, locking depth, and recurrence time are shown in figures 6 and 7. The residual velocities (GPS - model) are shown in figure 8 and the fit to the triangulation data is shown in figure 9.

The slip rates are in general good agreement with the prior distributions although the standard deviation of the posterior distributions is about half the prior standard deviation. This indicates that the estimates of slip rate from geology that have been adopted by the USGS for WGCEP are consistent with our estimate that incorporates geodetic data. The recurrence times are not well resolved as indicated by the similarity of the prior and posterior distributions in figure 7.

It is notable that the fit the strain rates at Pt. Reyes is quite good while the fit at Pt. Arena is poor. This was noted in previous 2D earthquake cycle studies. The inability of the model to fit the rapid post-1906 earthquake transient at Pt. Arena probably reflects the need for more than one relaxation mechanism (example afterslip) or nonlinear flow rheology at depth.

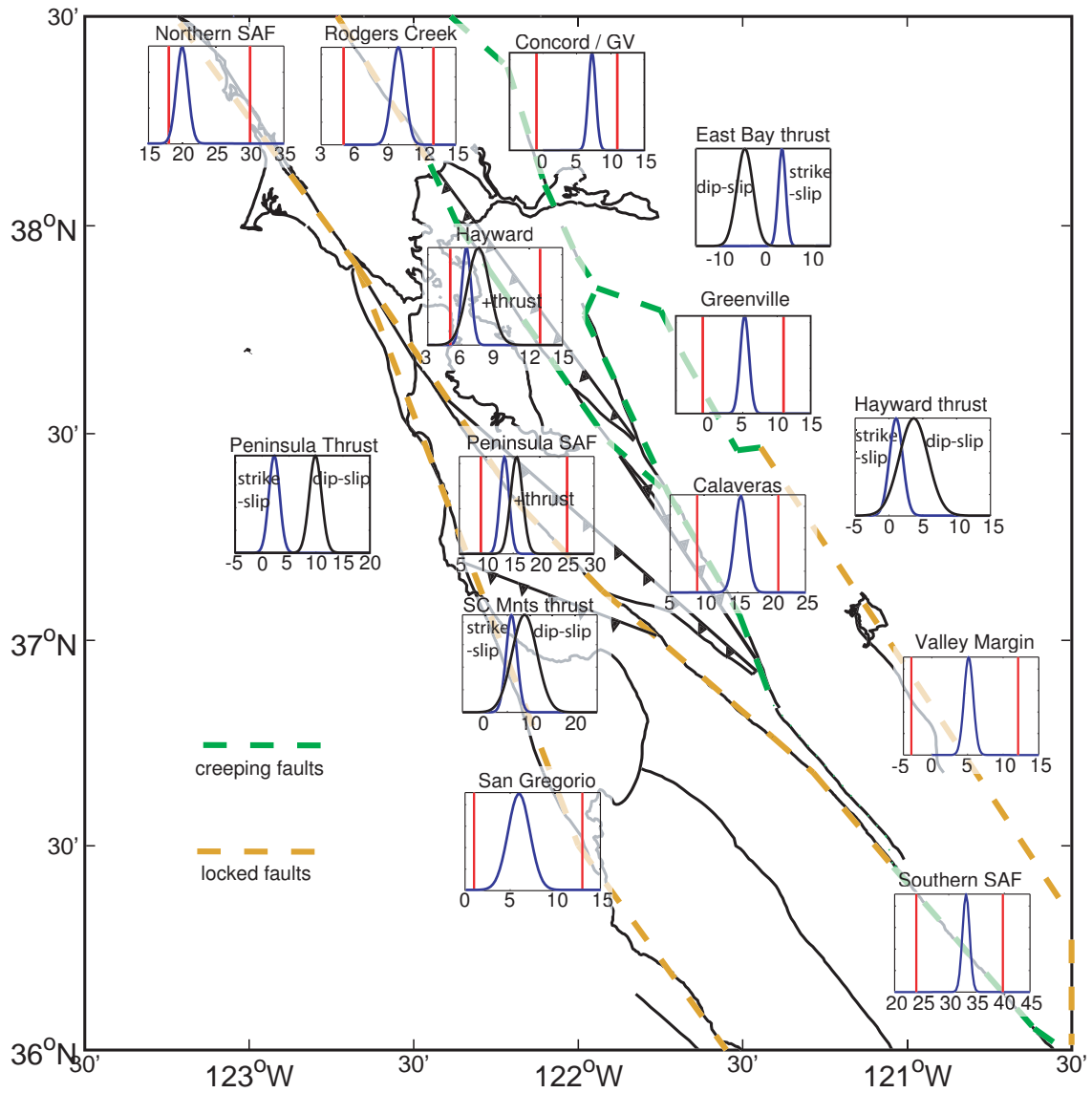


Figure 5: Posterior distributions for slip rate. Red vertical lines show  $2\sigma$  intervals for the prior.

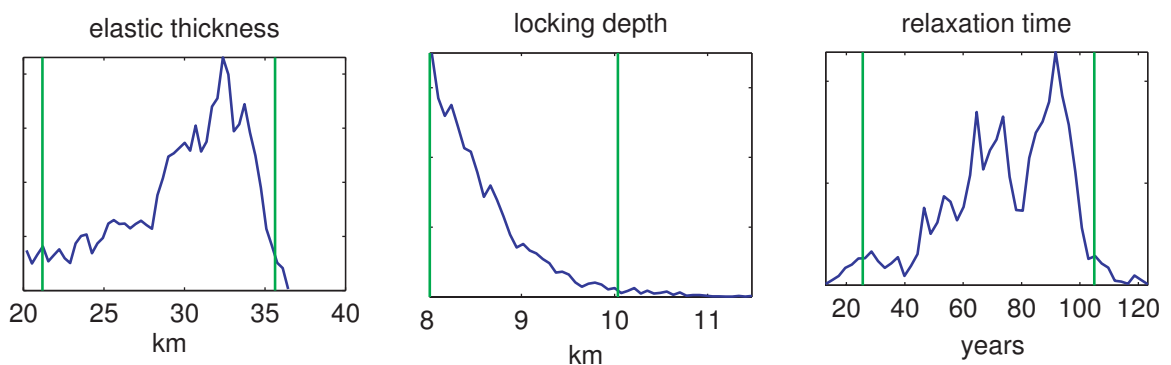


Figure 6: Posterior distributions for elastic thickness, relaxation time, and locking depth.

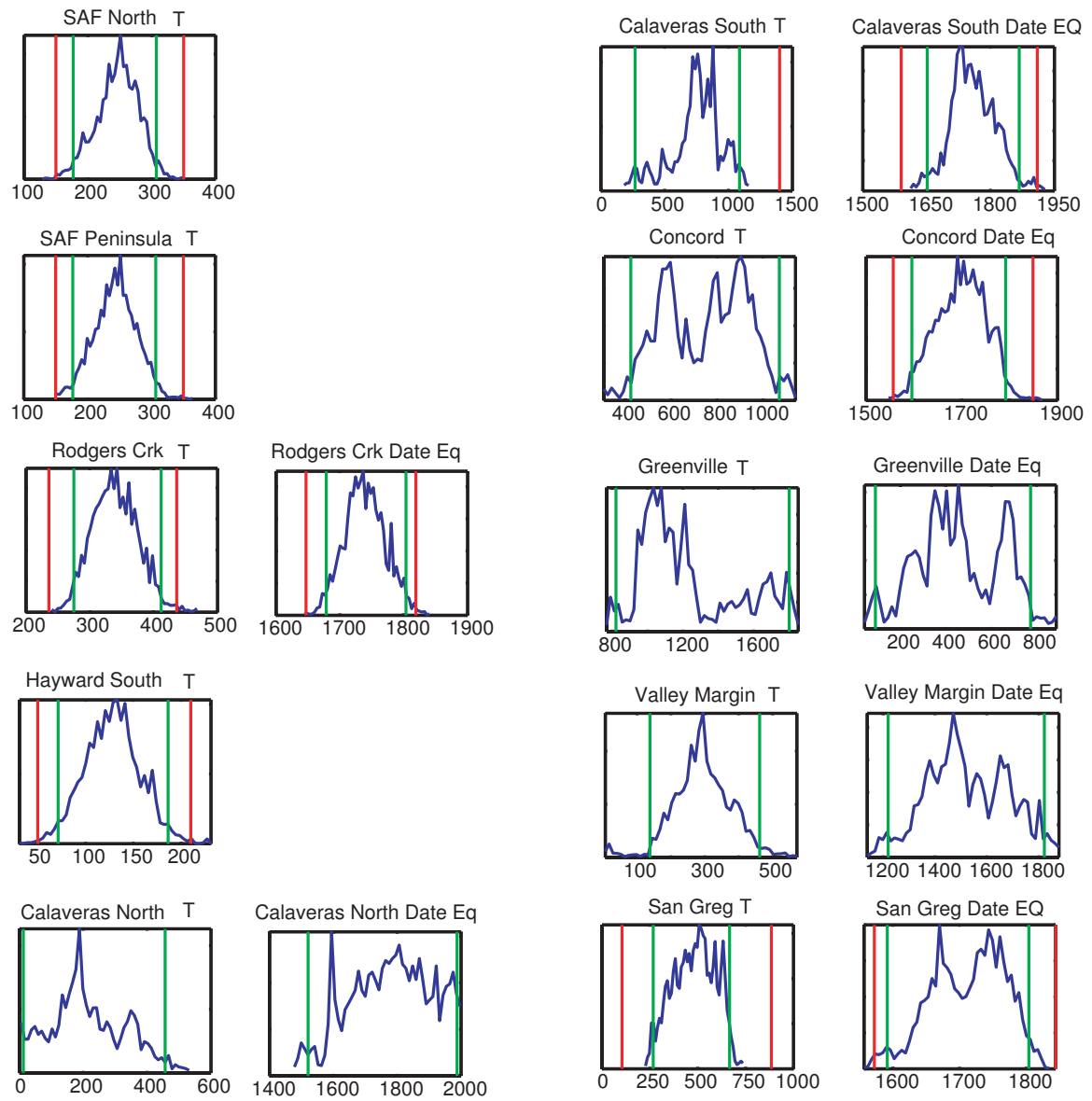


Figure 7: Posterior distributions for recurrence times..

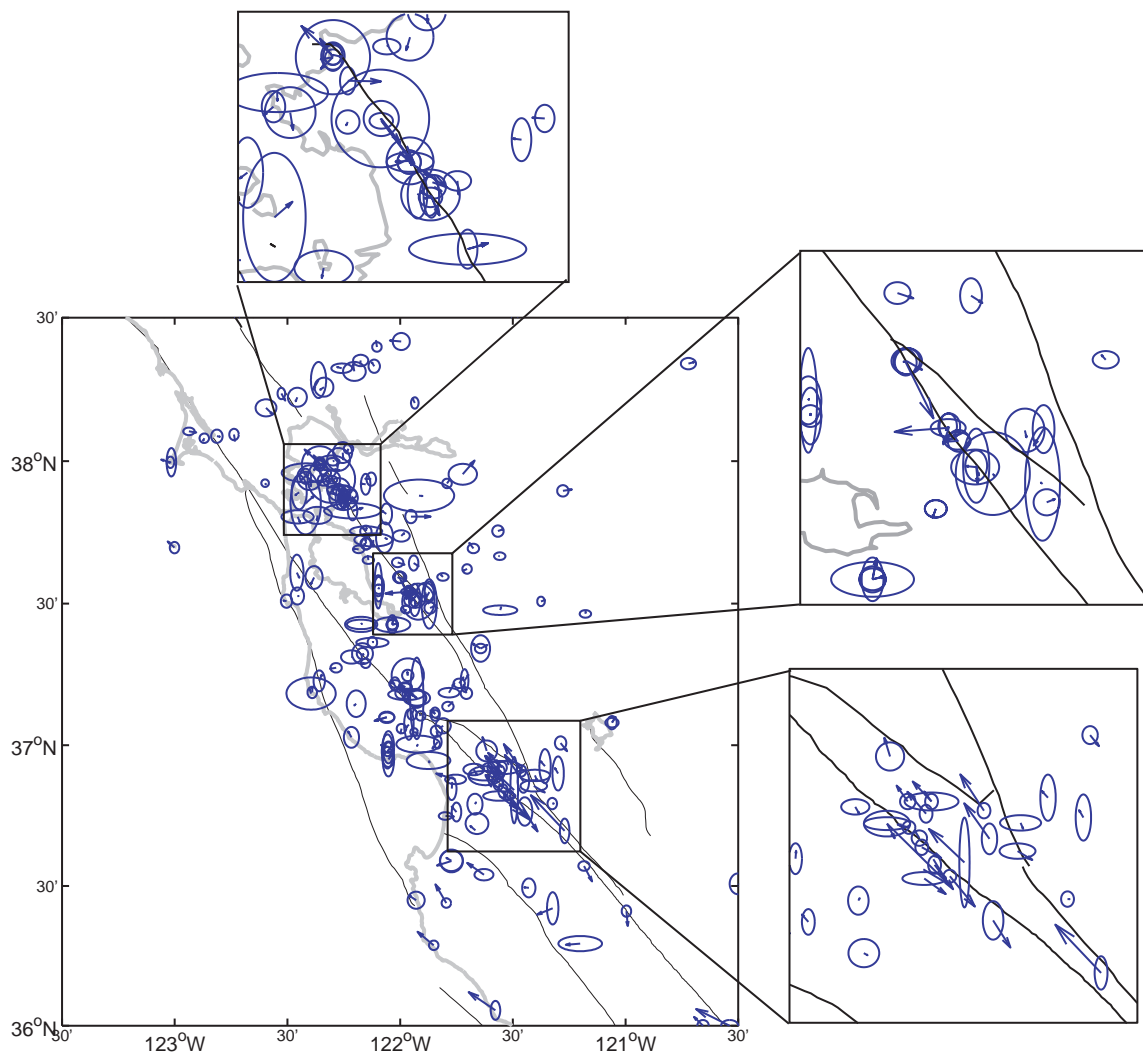


Figure 8: Residual velocities (GPS - model).

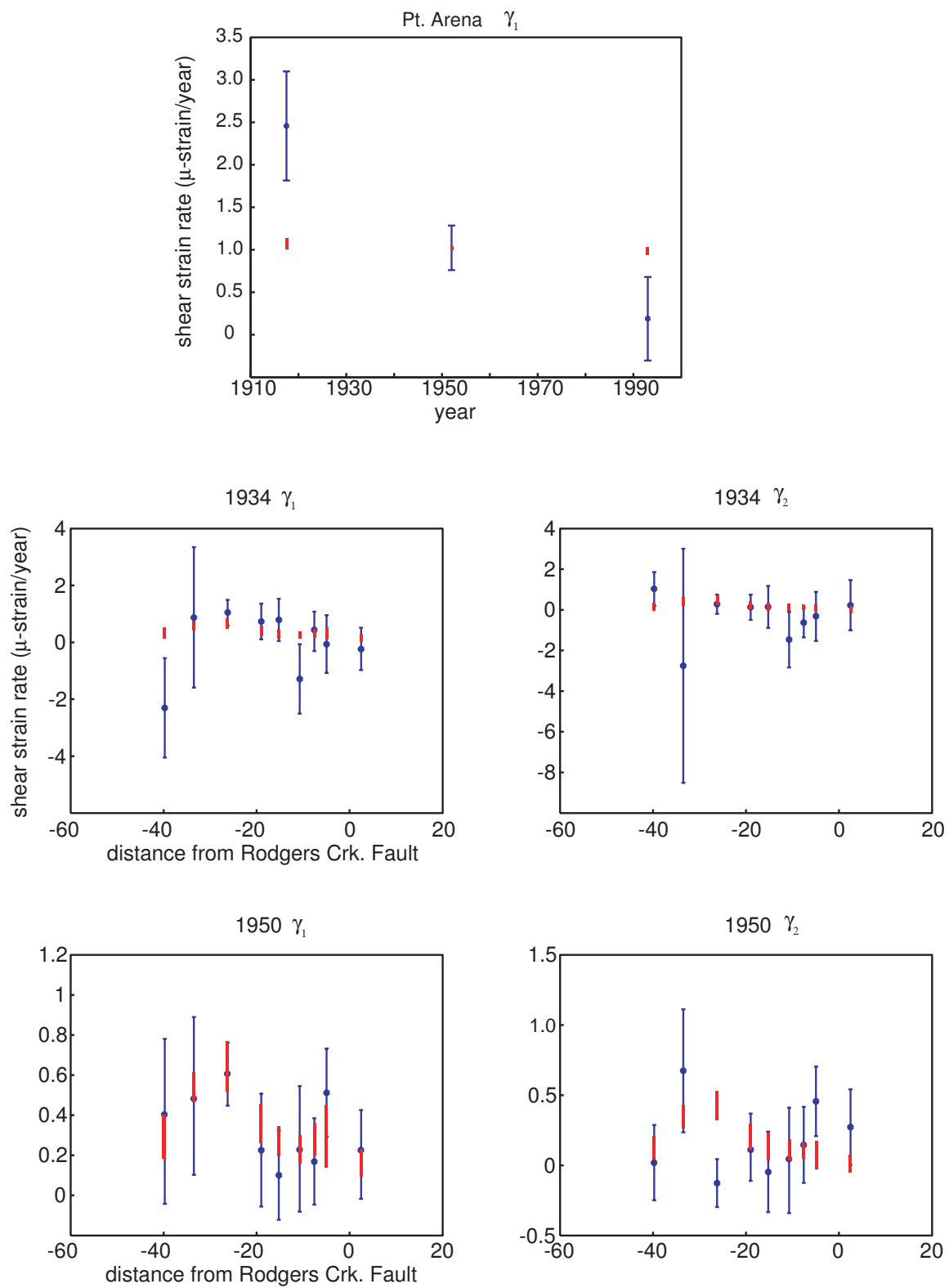


Figure 9: Fit to the triangulation data.

# Bibliography

- [1] Johnson K.M., Fukukda, J., and P. Segall, Distribution of Slip on San Francisco Bay Area Faults, *Eos Trans. AGU*, 87(52), Fall Meet. Suppl., Abstract G42A-06, 2006.
- [2] Fukuda, J., and K.M. Johnson, Estimating spatial distribution of slip with kinematic and hybrid-mechanical/kinematic block models: Application to San Francisco Bay Area faults (Abstract), SCEC Annual Meeting, 2006.
- [3] Johnson, K.M., and J. Fukuda, A 3D Viscoelastic Earthquake Cycle Model of Deformation in the San Francisco Bay Area (Abstract), SCEC Annual Meeting, 2006.